

Flux of atmospheric muons: Comparison between AIRES simulations and CAPRICE98 data.

P. Hansen, P. Carlson, E. Mocchiutti

Royal Institute of Technology (KTH),

AlbaNova University Center

S-10691 Stockholm,

Sweden.

S. J. Sciutto

Departamento de Física

Universidad Nacional de La Plata

C. C. 67 - 1900 La Plata

*Argentina.**

M. Boezio

University of Trieste and Sezione INFN di Trieste

Via A. Valerio 2

I-34147 Trieste

Italy

(Dated: 8th July 2003)

Abstract

We report on a comparison between the flux of muons in the atmosphere measured by the CAPRICE98 experiment and simulations performed with the air shower simulation program AIRES. To reduce systematic uncertainties we have used as input the primary fluxes of protons and helium nuclei also measured by the CAPRICE98 experiment. Heavy nuclei are also taken into account in the primary flux, and their contribution to the muon flux is discussed. The results of the simulations show a very good agreement with the experimental data, at all altitudes and for all muon momenta. With the exception of a few isolated points, the relative differences between measured data and simulations are smaller than 20 %; and in all cases compatible with zero within two standard deviations. The influence of the input cosmic ray flux on the results of the simulations is also discussed. This report includes also an extensive analysis of the characteristics of the simulated fluxes.

PACS numbers: 96.40.De, 96.40.Pq, 96.40.Tv, 02.70.Rr

*Fellow of Consejo Nacional de Investigaciones Científicas y Técnicas of Argentina.

I. INTRODUCTION

Detailed measurements and studies of the flux of muons in the atmosphere represent a subject of particularly great interest. This is mainly due to the fact that a measurement of the muon flux is an indirect measure of the neutrino flux and can therefore be used to improve the calculation of the atmospheric neutrino flux which in turn is used to compare with the observed neutrino rates in experiments targeted to detect neutrino oscillations. In addition, comparing measurements of fluxes of muons and other particles at different altitudes with simulated data is a powerful tool to check and/or calibrate air shower simulation programs. Such programs are not only essential to predict the atmospheric neutrino flux, but also play an important role in the analysis of data taken at highest energy air shower experiments like Auger [1], AGASA [2] or HiRes [3]. They are also used in Čerenkov light detector experiments like AMANDA [4] or ANTARES [5] to estimate backgrounds from atmospheric neutrinos.

Several calculations of the atmospheric muon flux at different altitudes have been performed in the past [6–8]. At ground level more data is available allowing also for simultaneous absolute flux and μ^+/μ^- flux ratio analysis [9–11]. The comparisons with experimental data show discrepancies in particular at low rigidities. The most significant differences between simulated and real data can be attributed to the following effects:

- The normalization of the primary cosmic ray flux. Different measurements disagree in about 10 % or more on the proton and helium spectra between 10 and 50 GeV [6].
- The solar modulation, the geomagnetic effect and the model of the atmospheric profile.
- The uncertainties in the particle production models, particularly the hadronic interaction generators [12].

The recent introduction of Ring Imaging Čerenkov counters (RICH) in balloon-borne spectrometers has made it possible to measure in the large proton background also positive muons. The CAPRICE98 experiment with a gaseous RICH [13], measured the flux of positive (negative) muons with momenta in the range 0.3-20 GeV/ c (0.3-40 GeV/ c), at different altitudes ranging from ground level (885 g/cm² atmospheric overburden) up to float altitude (5.5 g/cm²).

In this work we make a comparison between the direct measurement of the flux of muons in the atmosphere by the CAPRICE98 experiment [13] and the corresponding simulated values obtained from the air shower simulation program AIRES [14]. This program is a 3D Monte Carlo simulator where the majority of the processes that may undergo the shower particles, are taken into account. AIRES also has the advantage of including effects of the curvature of the Earth and of the geomagnetic field. The AIRES program has the possibility to swap between different hadronic models and it includes links to two well-known external hadronic interaction packages, namely SIBYLL [15] and QGSJET [16].

This paper is organized as follows: In section II we give some details of the CAPRICE experiment. In section III we report on the method used to simulate the muon flux, using as input experimental values for the cosmic ray fluxes at the top of the atmosphere (TOA). The results of the comparison between experiment and simulations are reported in section IV and finally we summarize our conclusions in section V.

II. THE EXPERIMENT

The analysis presented in this work use the muon fluxes measured by the CAPRICE98 (Cosmic Anti-Particle Ring Imaging Čerenkov Experiment) experiment, at all the atmospheric depths given in table I [13]. A detailed description of the procedures for muon identification, a careful study of the efficiency of each detectors, the various sources of background, and the rejection criteria and surviving contamination, can also be found in [13].

The balloon was launched from Ft. Summer, New Mexico, USA (34.28°N, 104.14°W) on the 28th May 1998 [17]. The following measurements were performed:

- **Muon measurement at ground.** Before launch the spectrometer took data at ground level for a period of about 14 hours. The ground level at Ft. Summer is located at an altitude of 1270 m that corresponds to an atmospheric depth of 885 g/cm².
- **Muon measurement during balloon ascending period.** During the ascent period of a few hours measurements were done on the flux of particles as a function of momentum and atmospheric depth.
- **Muon measurement during balloon floating period.** During the 20 hours at

<i>Level</i>	<i>Depth range (g/cm²)</i>	
	<i>min-max</i>	<i>average</i>
<i>ground</i>	885 – 885	885
10	581 – 885	704
9	380 – 581	462
8	250 – 380	308
7	190 – 250	219
6	150 – 190	165
5	120 – 150	136
4	90 – 120	104
3	65 – 90	77
2	33 – 65	48.4
1	15 – 33	22.6
<i>float</i>	5.45 – 5.95	5.5

Table I: Atmospheric depth intervals defined for CAPRICE 98.

float above 35 km, corresponding to approximately 5 g/cm² of residual atmosphere, the balloon spectrometer recorded data on muons, protons and helium nuclei. This last portion of the flight is important because it provides the data used to estimate the primary flux of proton and helium nuclei at the top of the atmosphere used in the simulations.

At every altitude the experimental data available includes the μ^+ (μ^-) flux for rigidities ranging from 0.3 GV up to 20 (40) GV. It is important to stress that this is the first experiment able to measure positive muons up to 20 GV. In the previous CAPRICE94 balloon flight [12, 18] the upper limit for μ^+ was 2 GV.

The CAPRICE98 spectrometer accepts particles arriving with an inclination with respect to the vertical axis of less than 20°. This characteristic of the instrument needs to be taken into account when performing a simulation. It is important to point out that the axis of the spectrometer remained vertical during the flight.

III. THE SIMULATIONS

A. Flux at the top of the atmosphere

The main input for the simulation of the flux of atmospheric muons at a given altitude is the absolute flux of cosmic rays at the top of the atmosphere. In the calculation we included the fluxes of the following 11 cosmic nuclei: H (protons and deuterium), He (He^3 and He^4), C, N, O, Ne, Mg, Si, and Fe.

The most important contribution to the total absolute flux at the top of the atmosphere comes from hydrogen and helium nuclei with only small contributions from other nuclei. It is also important to mention that photons and electrons do not contribute significantly to the flux of muons and therefore have not been included in our input.

We have mainly used hydrogen and helium fluxes obtained by the CAPRICE98 experiment [19], thus ensuring that the bulk of the input flux is affected by similar systematic errors as all the secondary particles, in particular muons, since all of them are measured with the same apparatus. This implies that when comparing experimental data at a given atmospheric depth with the corresponding simulations, a direct evaluation of the properties of the propagating algorithms is being performed, minimizing the uncertainty due to any inaccuracies in the input flux.

The CAPRICE98 experiment measured the absolute flux of cosmic protons (helium nuclei) with kinetic energies ranging from 3 to 350 GeV (0.9 to 170 GeV/nucleon) [19]. These absolute fluxes can be adequately parameterized as polynomial functions of the logarithm of the primary energy. The deuterium to proton and He^3 to He^4 ratios were taken from reference [20]. For heavier nuclei we have used data from reference [21].

The absolute TOA fluxes of hydrogen (proton + deuterium), helium ($\text{He}^3 + \text{He}^4$), carbon, oxygen, and iron are shown as functions of the energy of the primary particles in figure 1. The lines represent the polynomial functions used as input for the simulations. The CAPRICE98 proton and helium data are also shown. The parameterized representations agree excellently with the experimental data.

It is important to remark that for low energies (below about 3 GeV) the solar modulation was taken into account when fitting the plotted functions, considering the level of solar activity registered at the date of the CAPRICE98 flight.

Notice also that the input fluxes used in the simulations correspond to total absolute fluxes at TOA without any correction due to geomagnetic effects. Such effects are taken into account by the simulation and analysis chain used to evaluate the different simulated observables: a corrective weight is applied to the secondaries generated by each primary entering the atmosphere to effectively take into account the geomagnetic cutoff. Then, the particles are propagated within the atmosphere, also taking into account their deflections due to the geomagnetic field, which is in this case taken as constant.

B. Air shower simulations

The AIRES simulation engine [14, 22] provides full space-time particle propagation in a realistic environment, taking into account the characteristics of the atmospheric density profile (using the standard US atmosphere [23]), the Earth's curvature, and the geomagnetic field (calculated for the location and date of the CAPRICE98 flight with an uncertainty of a few percent [24]).

The following particles are taken into account in the AIRES simulations: photons, electrons, positrons, muons, pions, kaons, eta mesons, lambda baryons, nucleons, antinucleons, and nuclei up to $Z = 36$. Nucleus-nucleus, hadron-nucleus and photon-nucleus inelastic collisions with significant cross-sections are taken into account in the simulation. The hadronic processes are simulated using different models, accordingly to the energy: high energy collisions are processed invoking an external package (SIBYLL 2.1 [15] or QGSJET01 [16]), while low energy ones are processed using an extension of Hillas splitting algorithm (EHSA) [22, 25, 26]. The threshold energies separating the low and high energy regimes used in our simulations are 200 GeV and 80 GeV for the SIBYLL and QGSJET cases, respectively. The EHSA low energy hadronic model used in AIRES is a very fast procedure, effectively emulating the major characteristics of low energy hadronic collisions. The model is adjusted to retrieve similar results as the high energy hadronic model for energies near the transition thresholds previously mentioned, and the low energy cross sections are calculated from parameterizations of experimental data. A complete discussion on the low energy hadronic models is clearly beyond the scope of this paper. A separate report on this subject will be published elsewhere [27].

AIRES has been successfully used to study several characteristics of high energy showers,

including comparisons between hadronic models [26, 28], influence of the LPM effect [29], muon bremsstrahlung [30], and geomagnetic deflections [24] on the shower development. AIRES has also been used to obtain an energy calibration of the AGASA experiment [31], and to study the expected efficiency of the Auger Observatory for detecting quasi-horizontal showers generated by τ -neutrinos [32].

In the present work, AIRES has been used to simulate showers with primary energies from 7.5×10^8 up to 10^{15} eV. In order to accurately simulate the absolute fluxes already described in section III A, and also to optimize the statistics, we conveniently divided the primary energy range into many subintervals with boundaries chosen so as to have at each of them approximately constant compositions and slope γ ($\gamma = d\Phi/dE_{pr}$ where Φ is the flux and E_{pr} is the primary energy). The independent sets of simulated showers were generated for each one of the intervals, considering also an isotropic arrival direction distribution with zenith angles ranging from 0° to 89° .

The shower simulations performed for this study add up to more than 300 millions of showers, generating particle data files with a total size of about 30 GB, and requiring about 20 days of processing time (using a 1 GHz processor). The generation of such large set of simulated showers proved to be a straightforward computing exercise, where the AIRES system could be easily configured for this particular task, even if it was originally designed to simulate showers with significantly larger energies.

When configuring the simulation program, several aspects have been taken into account to properly set up the input parameters in our case of flux simulation. In particular, we would like to make the following remarks: (i) The low energy hadronic interactions increase their importance as the primary energy decreases. For this reason, we have done a careful setting of the parameters of the EHSA, taking into account experimental results, and comparisons with other models. (ii) The statistical sampling algorithm of AIRES (the so-called thinning) [14] was completely disabled. This means that all the secondaries generated during the shower development are fully propagated. (iii) All electromagnetic particles (photons, electrons, and positrons) with energies below 100 MeV were discarded. This significantly reduces the processing time required for a given simulation, without altering the propagation of hadrons and muons.

C. Simulating the flux of secondary particles.

Let us consider a given observing level located at an altitude h smaller than the injection altitude h_i . After simulating the shower in the conditions of section III A, the secondary particles arriving to the observing level, are processed to estimate the corresponding fluxes, according to the following conditions:

- When comparing with CAPRICE98 measurements [13], only particles reaching the observing level with an inclination of less than 20° have been considered. In this paper all particles satisfying that selection criterion are referred as *quasi-vertical* particles. Unless otherwise specified all the results discussed in the following sections apply to quasi-vertical particles. Notice also that *full* fluxes refer to fluxes of particles coming from all directions.
- When necessary, the selected secondary particles are binned according to their momenta, using the momentum intervals of the experimental data.
- The selected particles are weighted to take into account the absolute flux normalization associated with the primary energy subinterval (see section III A) that corresponds to the shower being analyzed.

The procedure to evaluate the fluxes is repeated at each of the observing altitudes that are considered, using at each altitude an independent set of simulated showers.

IV. RESULTS

A. General analysis of the simulated flux

The fluxes of secondary particles have been simulated for all altitudes listed in table I. We have also performed simulations at sea level (1035 g/cm^2). In figure 2 the total fluxes of muons, pions, protons, neutrons and helium nuclei are plotted as function of atmospheric depth and altitude above sea level. Electrons, positrons and photons were not propagated in detail in the simulation (see section III) and are therefore not considered in our study. Some of the main characteristics of these particle fluxes show up in this figure. At the highest level (5.5 g/cm^2) protons are the most abundant particles because only a small fraction

of them have interacted. On the other hand, at altitudes near sea level, the total flux is dominated by muons, which account for more than 96 % of the considered particles. Notice also that, as expected, the muon flux increases with decreasing altitude, until reaching a maximum around $X = 150 \text{ g/cm}^2$. The muon flux then decreases with decreasing altitude until sea level. For atmospheric depths in the range $90 - 300 \text{ g/cm}^2$ the flux of muons is quite constant. The pion flux behaves similarly, reaching its maximum approximately at the same altitude as that for the muons.

We have studied how the different primaries that make up the primary flux at the TOA, already described in section III A, contribute to the total muon flux at different altitudes. In figure 3 the relative contributions of proton, helium nuclei, and other heavy nuclei (C, N, O, Ne, Mg, Si, Fe) to the muon flux are plotted versus atmospheric depth and altitude above sea level. It is evident that protons give the largest contribution at all altitudes, and their contribution increases when the altitude decreases. The heavy nuclei contribute with a small but not completely negligible fraction that ranges from about 8 % at sea level up to more than 10 % at $X = 5.5 \text{ g/cm}^2$.

The contributions to the flux of muons with momenta larger than $10 \text{ GeV}/c$ is also displayed (open symbols) in figure 3. The different fractions are similar to the corresponding ones for the total muon flux, except at high altitudes where the proton fraction is substantially larger in comparison with the previous case.

It is also interesting to analyze how primaries with different energies (for nuclei total kinetic energy) contribute to the muon flux. To this end, we have divided the primary energies E_{pr} into four ranges, namely, (1) $E_{pr} < 10 \text{ GeV}$; (2) $10 \text{ GeV} < E_{pr} < 100 \text{ GeV}$; (3) $100 \text{ GeV} < E_{pr} < 1 \text{ TeV}$; and (4) $E_{pr} > 1 \text{ TeV}$. The corresponding contributions to the muon flux using the data of our simulations are displayed in figure 4, where the relative contributions of each of the four primary energy categories to the full muon flux (including all arrival directions) are plotted versus atmospheric depth and altitude. As expected, in the energy range 10-100 GeV primaries, that account for the most significant fraction of particles capable of entering into the Earth's atmosphere, are the ones that contribute most to the muon flux at all altitudes. Lower energy primaries contribute significantly (30 to 40 %) only at high altitudes, but their contribution decreases rapidly for X longer than 100 g/cm^2 . Near sea level, the contributions of energy range 3 and 4 primaries increases significantly with a contribution from 100 GeV -1 TeV primaries of more than 30 % (20 % when selecting only

quasi-vertical muons). We have studied the contribution of very low energy primaries ($E_{pr} < 3$ GeV) (the results have not been included in figure 4 for simplicity). Their contribution to the flux is always small ($< 1.5\%$) in the entire range of altitudes considered. This implies that any errors in the estimation of the input flux for very low energies are unlikely to have a significant impact on the simulated muon fluxes (notice that 3 GeV is the lowest primary energy measured by CAPRICE98).

To complete our study of how the different primary particles contribute to the flux of muons at different altitudes, we have analyzed the number of muons generated from primaries with given zenith angles. The results of this analysis are displayed in figures 5 and 6.

In figure 5 the relative contributions to the full flux of muons corresponding to primaries with zenith angle, Θ , less than 30° (circles), greater than 30° and less than 60° (squares), and greater than 60° (triangles), are plotted versus atmospheric depth and altitude. The solid (open) symbols correspond to all muons (muons with momentum larger than 10 GeV/c).

The curves in this figure present a complicated dependency on altitude of the corresponding contributions. At sea level, showers with $30^\circ < \Theta < 60^\circ$ dominate the contribution of the full flux, and the different contributions are independent of the muon momentum. At high altitudes the contribution of very inclined showers is dominating. This is due to the fact that such showers pass through a thicker layer of air and are more developed and producing more muons before reaching observation level, in comparison with vertical ones (see the discussion on angular distributions of muons later in this section). This effect is more important in the case of high energy muons, as indicated by the open symbol curves.

This picture changes dramatically when considering only quasi-vertical muons, as displayed in figure 6. In this case the showers with $\Theta < 30^\circ$ are the ones that most contribute at all altitudes, and their relative contribution is larger for high energy particles, reaching virtually 100 % when selecting muons with momenta greater than 10 GeV/c. Notice that in figure 6 the open circles correspond to muons with momenta larger than 1 GeV/c.

Another very important observable that we have considered in our analysis, is the distribution of arrival directions of muons at different altitudes. As we have already commented in section II, and as explained in detail in reference [13], the normalization of the muon fluxes measured by CAPRICE98 is calculated under the assumption of an isotropic distribution of muons within the acceptance cone (zenith angle less than 20°). In order to check the validity of this assumption, we have recorded angular distributions of muons at all the simulated

levels and, simultaneously, calculated the fluxes using several aperture cones.

To start with, let us consider the angular distributions of all atmospheric muons. In figure 7 the normalized angular distributions of muons are plotted versus the cosine of the arrival zenith angle in the entire $[0, 1]$ range for several altitudes namely (a) 5.5 g/cm^2 , (b) 77 g/cm^2 , (c) 308 g/cm^2 , and (d) 885 g/cm^2 .

We have found that in the entire range of altitudes considered the angular distributions can be accurately fitted by the following function:

$$f(\cos \theta) = U (\cos \theta)^{(\alpha + \beta \cos \theta)} \quad (1)$$

where α and β are constants, and U is a normalization factor determined by the condition $\int_0^1 f(x) dx = 1$. This function can be conveniently fitted, with α and β as free parameters, using simulated or experimental data.

The constants α and β vary slowly as function of the atmospheric depth of the observing level as illustrated in figure 8. Notice that for $x \sim 600 \text{ g/cm}^2$ $\beta \cong 0$, and therefore in this case the distribution reduces to a power of $\cos \theta$.

An important characteristic of the distributions plotted in figure 7 is that in the range $\theta < 20^\circ$ (corresponding to $\cos \theta > 0.94$) the variations as functions of angle are small, in particular for high altitudes. This implies that the isotropy hypothesis is reasonably justified and at the same time, the fluxes estimated using aperture cones smaller than, say, 20° , should not differ significantly.

This property shows up clearly from figures 9, 10 and 11 where the simulated μ^+ and μ^- fluxes calculated using different acceptance cones, are plotted versus muon momentum at atmospheric depths 22.6 , 308 , and 885 g/cm^2 , respectively. Notice that there are no important differences between the 10° and 20° cases.

From the distributions in figures 10 and 11 it is clear that the high momentum end of the spectra do not significantly depend on the aperture cone used. However, this is not the case for the distributions in figure 9 where it can be seen that the steepness of the distributions for large momenta decreases with aperture angle. This can be explained analyzing the angular distributions of high energy atmospheric muons. In figure 12, the angular distributions for (a) all simulated muons, (b) $p_\mu > 1 \text{ GeV}/c$, (c) $p_\mu > 10 \text{ GeV}/c$, (d) $p_\mu > 100 \text{ GeV}/c$, are shown for four different altitudes. We conclude from these figures that (i) the distributions for the lower altitudes, 5.5 and 77 g/cm^2 show a large variation in angular distribution for

different energies, (ii) at high altitudes $\theta = 0$ does no more correspond to the maximum of the distribution (d) which is located rather close to $\theta = 90^\circ$. Therefore, when enlarging the aperture angle an increasing number of muons is accepted, consequently producing a larger flux at high momenta.

It is worthwhile mentioning that this feature of the angular distribution of high energy muons at large altitudes implies that any experiment having a narrow acceptance cone centered at the vertical only accumulates a very small fraction of the muon flux.

B. Comparison with experimental data

We have compared the fluxes obtained by Monte Carlo simulations with the experimental data available at every altitude. Figures 13, 14 and 15 summarize the results obtained for the ascent, float and ground measurement phases, respectively. In these figures the fluxes of negative and positive muons are plotted as functions of the muon momentum for every altitude considered. In figure 13, that corresponds to the ascent phase of the CAPRICE98 flight, the fluxes corresponding to different altitudes have been multiplied by powers of 100, as indicated in the respective figure caption. The full lines correspond to the AIRES simulations; while the solid squares represent CAPRICE98 data. When available, CAPRICE94 data [12, 18] have been displayed as well (open triangles). Notice that the CAPRICE94 flight corresponds to a different geographical location, and a different time. Therefore the corresponding results, especially for low muon momenta, are not directly comparable to the simulations, that were performed taking into account the CAPRICE98 environment.

The shaded bands drawn together with each distribution illustrate how the flux changes inside the atmospheric depth intervals of table I. The varying width of these shaded areas can be understood taking into account the behavior of the total muon flux for varying atmospheric depth, represented in figure 2. Near the top of the atmosphere, the muon flux grows with X , and a visible difference between fluxes evaluated at the minimum and maximum depth of each measurement interval exists as made evident for all momenta in the highest levels plotted in figure 13. In these cases the lower (upper) curve of the shaded region corresponds to the respective minimum (maximum).

On the other hand, in the cases of measurement intervals located close to the ground

level, the muon flux decreases with X , and therefore the positions of the distributions corresponding to the minimum and maximum depth of the respective interval interchange with respect to the highest ones discussed in the previous paragraph. In these cases there are no important variations at the high energy end of such distributions.

For X ranging from about 70 g/cm² to about 200 g/cm² the muon flux remains approximately constant. In this case the curves corresponding to minimum, maximum and average depth for a given level overlap. As a consequence, any errors due to uncertainties in the altitude of the balloon and/or the atmospheric model used in the simulations should be very small at these intermediate depths.

The relative differences between simulated and experimental data, are shown in figure 16 as function of the atmospheric depth. For each atmospheric depth, the relative difference is a weighted average over momenta, where the weight is the inverse of the relative error on each measured point. The error bars have been calculated taking into account both the experimental and Monte Carlo errors. To estimate these last ones we have taken into account only the uncertainty derived from the uncertainty in the flux at TOA, whose average over the energies with measurements is around 10%. The Monte Carlo statistics is very large so statistical fluctuations of mean values can be neglected. We have not attempted in this work to do a detailed analysis of other uncertainties that can affect the simulated data.

The relative differences are generally compatible with zero within one standard deviation of the experimental flux. At float altitude the simulated flux for μ^+ is 38 ± 18 % above the measured one. At ground level the simulated flux is approximately 20 % lower than the experimental one.

The global averages of the relative differences, represented in figure 16 as dotted lines, are essentially zero (there is a slight positive tendency of about 5 % in the μ^- case, that is compatible with zero well within 1σ).

The ground level data is worth of a special analysis because in this case the flux was measured with high statistics, allowing for narrower momentum bins. The comparison between simulated and experimental data indicate that the simulations predict a flux that is smaller than the experimental one, especially for high muon momenta, even if such difference is compatible with zero within 2σ . There are several possible reasons for these differences, as already mentioned in the introduction. We discuss here some of our results.

The differences between simulated and experimental data at ground, amounting to about

20%, suggest that there are systematic errors on that level since the statistical errors are very small. The relative importance of primaries with energies above 100 GeV (see figure 4) is larger for ground data than for data at higher altitudes, suggesting that primary energy dependent systematic errors could have a non negligible effect on the muon data at ground. This will be the subject of a detailed study to appear later.

The study of the μ^+/μ^- flux ratio can also provide important information to test the models used in the simulations. We consider only the data at ground level where contamination corrections are negligible, and the experimental data is abundant enough to give small errors. In figure 17 the flux ratio at ground is plotted versus muon momentum. The squares (triangles) correspond to the CAPRICE98 (CAPRICE97) experimental data, while the shaded area represents the simulation results including an approximate estimation of modeling errors coming from different uncertainties (geomagnetic effects, input flux, hadronic models, etc.). It is worthwhile mentioning that the statistics of the CAPRICE97 data set is about four times larger than that of the CAPRICE98 case, resulting, as is evident from the plot, in smaller error bars. When comparing the results of the simulations with the experimental data, we find in general an acceptable agreement, with relative differences always located within 2σ . However, in the approximate range 3-40 GeV/c the simulations give ratios that are about 10% lower than the experimental results. Such differences are of the same order of magnitude than the ones reported in a similar study performed using various hadronic models [10], giving a qualitative indication of how much these models can change the simulated μ^+/μ^- flux ratio. A complete study of the impact of different hadronic models, as well as other factors that could influence the final simulated ratio is beyond the scope of this work, and will be addressed in a future publication.

It is also interesting to study the change with altitude of the flux of muons with a given momentum. In figure 18 the absolute fluxes of muons corresponding to each of the experimental momentum bins are plotted as functions of the atmospheric depth.

Those curves indicate that there exists a very good agreement between our simulations with AIRES and the experimental data in all the considered cases, with no evident bias of any kind. We also note that at each momentum bin both experimental and simulated curves have their maxima approximately at the same altitude.

V. CONCLUSIONS

An in depth analysis of the absolute flux of muons at different atmospheric depths has been performed. This includes a comparative study of fluxes measured by the CAPRICE98 and CAPRICE94 experiment with the corresponding simulations with AIRES. Additionally, the most important correlations between the simulated observables and different input parameters are discussed.

Many of the results presented in the previous sections indicate clearly that the strategy followed to perform the simulations is capable of producing acceptable results. We could also verify that the following conditions cannot be simplified without altering to some extent the simulated fluxes:

- Input fluxes that include H, He, and other heavy nuclei, with energies up to a maximum value of at least 10 TeV.
- Full 3d propagation of particles.
- Wide range of primary zenith angles, especially for simulation of full fluxes.

The fluxes simulated with AIRES present a very good agreement with the corresponding ones measured experimentally, at all altitudes and muon momenta considered. With the exception of a few isolated points, the relative differences between simulated and experimental data are always smaller than 20 %. In most cases the relative differences are compatible with zero within error bars. Global averages of relative differences are technically zero, and there are no evident bias that could indicate that the simulation algorithms are not performing adequately.

Detailed comparisons between measured and simulated atmospheric muon data are surely useful to tune the simulation program but requires experimental measurements substantially more accurate than the ones available at present. In this direction, the CAPRICE re-flight project [35] constitutes a very important effort capable of providing improved measurements that will allow the production of more detailed comparative analysis of real and simulated data.

VI. ACKNOWLEDGMENTS

One of the authors (S. J. S.) is indebted to Prof. Per Carlson and colleagues at the Department of Physics, KTH, Sweden, for their kind hospitality. This work was partially supported by CONICET and Fundación Antorchas of Argentina. P. H. thanks Roberto Liotta for useful discussion and the Swedish Foundation for International Cooperation in Research and Higher Education for support. E. M. was supported by the Foundation BLANCEFLOR Boncompagni-Ludovisi, née Bildt.

-
- [1] <http://www.auger.org>
 - [2] <http://www-akeno.icrr.u-tokyo.ac.jp/AGASA/results.html>
 - [3] <http://hires.physics.utah.edu>
 - [4] <http://amanda.uci.edu>
 - [5] <http://antares.in2p3.fr>
 - [6] V. A. Naumov, hep-ph/0201310.
 - [7] G. Battistoni, A. Ferrari, T. Montaruli, P. R. Sala, hep-ph/0107241
 - [8] R. Engel, T. K. Gaisser, and T. Stanev, *Proc. 27th ICRC (Hamburg)*, **1**, 1029 (2001).
 - [9] B. Vulpescu, *et al.*, *J. Phys. G*, **27**, 977 (2001).
 - [10] J. Wentz, *et al.*, *Proc. 27th ICRC (Hamburg)*, **1**, 1167 (2001).
 - [11] J. Wentz, *et al.*, *Phys. Rev. D*, **67**, 073020 (2003).
 - [12] M. Boezio, *et al.*, *Phys. Rev. Lett.*, **82**, 4757 (1999).
 - [13] M. Boezio, *et al.*, *Phys. Rev. D*, **67**, 072003 (2003).
 - [14] S. J. Sciutto, AIREX User's Manual and Reference Guide; version 2.6.0 (2002), available electronically at www.fisica.unlp.edu.ar/auger/aires.
 - [15] R. Engel, T. K. Gaisser, T. Stanev, *Proc. 26th ICRC (Utah)*, **1**, 415 (1999).
 - [16] N. N. Kalmykov and S. S. Ostapchenko, *Yad. Fiz.*, **56**, 105 (1993); *Phys. At. Nucl.*, **56**, (3) 346 (1993); N. N. Kalmykov, S. S. Ostapchenko and A. I. Pavlov, *Bull. Russ. Acad. Sci. (Physics)*, **58**, 1966 (1994).
 - [17] M. Ambriola *et al.*, *Nucl. Phys. B Proc. Suppl.*, **78**, 32 (1999).
 - [18] M. Boezio, *et al.*, *Phys. Rev. D*, **62**, 032007 (2000).

- [19] M. Boezio, *et al.*, *Astropart. Phys.*, **19**, 583 (2003).
- [20] J. Z. Wang, *et al.*, *Proc. 27th ICRC (Hamburg)*, **5**, 1671 (2001).
- [21] P. K. F. Grieder, *Cosmic Rays at Earth*, Elsevier (2001), Chapter 5.
- [22] S. J. Sciutto, *Proc. 27th ICRC (Hamburg)*, **1**, 237 (2001).
- [23] National Aerospace Administration (NASA), National Oceanic and Atmospheric Administration (NOAA) and US Air Force, US standard atmosphere 1976, NASA technical report NASA-TM-X-74335, NOAA technical report NOAA-S/T-76-1562(1976).
- [24] A. N. Cillis, S. J. Sciutto, *J. Phys. G*, **26**, 309 (2000).
- [25] S. J. Sciutto, J. Knapp, D. Heck, *Proc. 27th ICRC (Hamburg)*, **1**, 526 (2001).
- [26] J. Knapp, D. Heck, S. J. Sciutto, M. T. Dova, M. Risse, *Astrop. Phys.*, **19**, 77 (2003).
- [27] S. J. Sciutto, in preparation.
- [28] L. A. Anchordoqui, M. T. Dova, L. N. Epele, S. J. Sciutto, *Phys. Rev. D*, **59**, 094003 (1999).
- [29] A. N. Cillis, H. Fanchiotti, C. A. García Canal, S. J. Sciutto, *Phys. Rev. D*, **59**, 113012 (1999).
- [30] A. N. Cillis, Sciutto, S. J., *Phys. Rev. D*, **64**, 013010 (2001).
- [31] N. Sakaki, *et al.*, *Proc 27th ICRC (Hamburg)*, **1**, 329 (2001).
- [32] X. Bertou, P. Billoir, O. Deligny, C. Lachaud, A. Letessier-Selvon, *Astropart.Phys.*, **17**, 183 (2002).
- [33] S. Swordy, *et al.*, *Astrophys. J.*, **403**, 658 (1993).
- [34] D. Müller, *et al.*, *Astrophys. J.*, **374**, 356 (1991).
- [35] M. Circella, *et al.*, *Proc. 27th ICRC (Hamburg)*, **1**, 1251 (2001).
- [36] J. Kremer, *et al.*, *Phys. Rev. Lett.*, **83**, 4241 (1999).

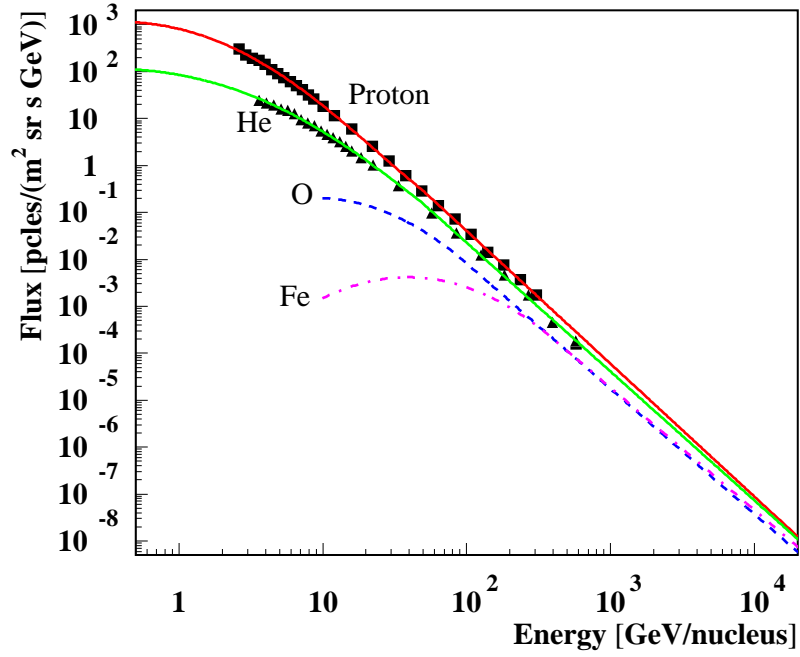


Figure 1: Absolute fluxes of proton, helium, carbon, oxygen, and iron nuclei at the top of the atmosphere, plotted as functions of the kinetic energy of the primary. The points represent data from the CAPRICE98 experiment [19], in the cases of proton (squares) and helium nuclei (triangles). The lines are the polynomial functions discussed in the text.

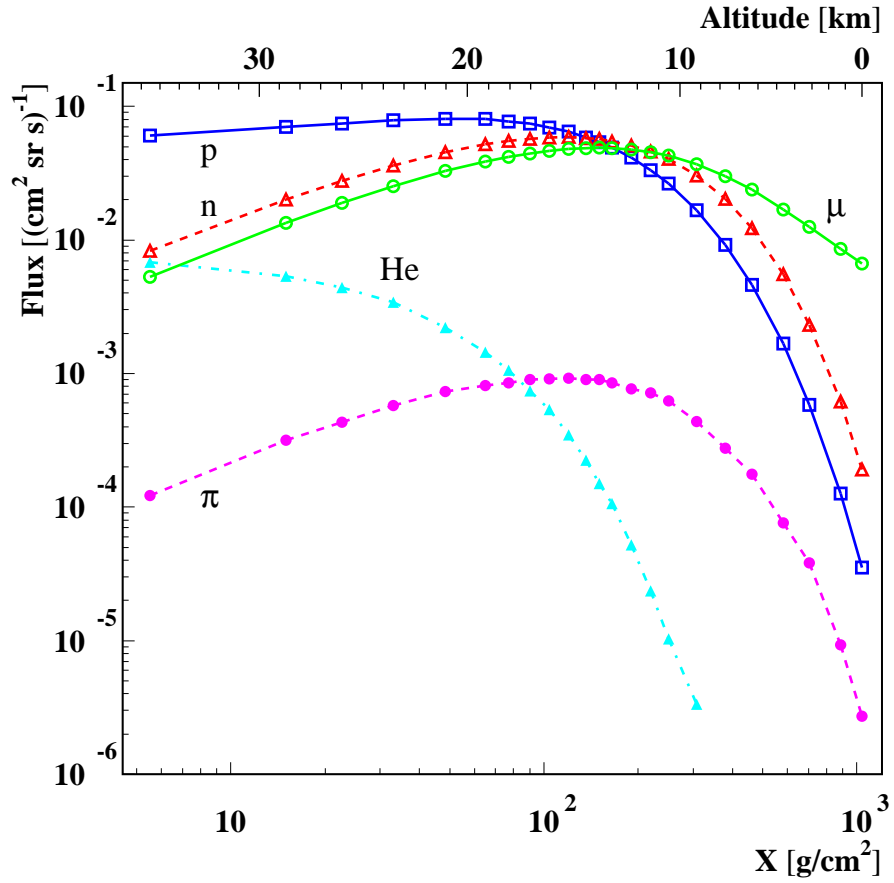


Figure 2: Total fluxes of muons, pions, protons, neutrons and helium nuclei as a function of atmospheric depth and altitude above sea level. The lines are drawn to guide the eye.

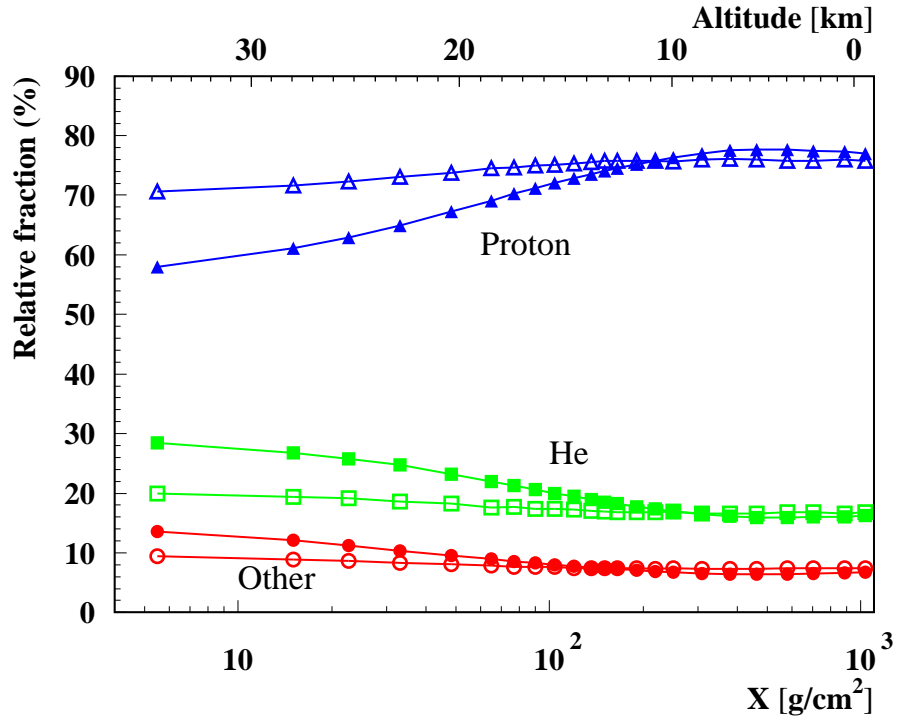


Figure 3: Relative contributions of different primary particles to the full muon flux as function of atmospheric depth and altitude above sea level. The solid (open) symbols correspond to all muons (muons with momentum greater than 10 GeV/c). The lines are drawn to guide the eye.

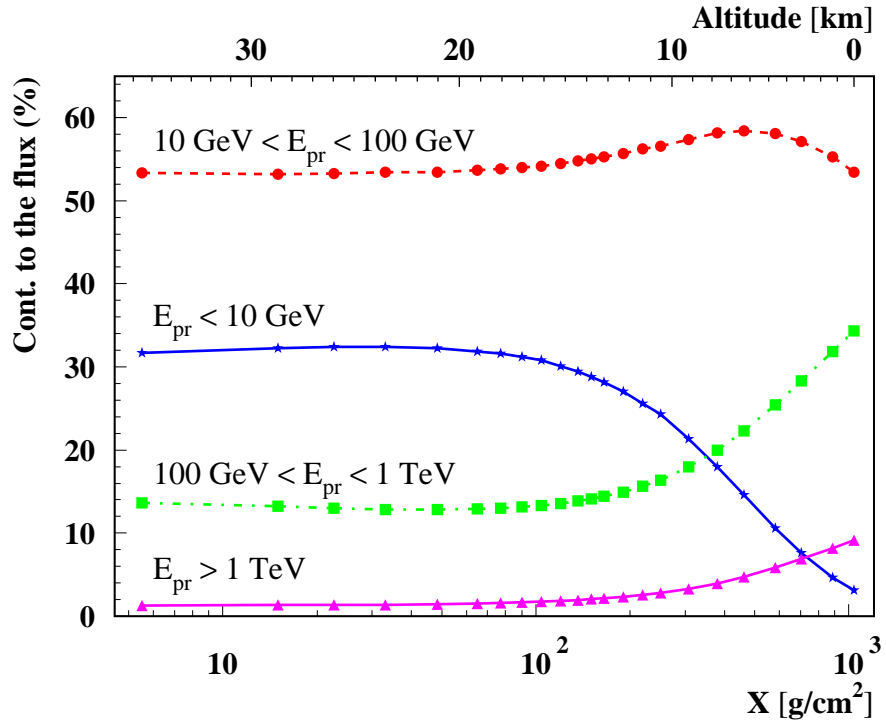


Figure 4: Relative contribution of primaries with different energies to the full muon flux as function of atmospheric depth and altitude above sea level. The lines are drawn to guide the eye.

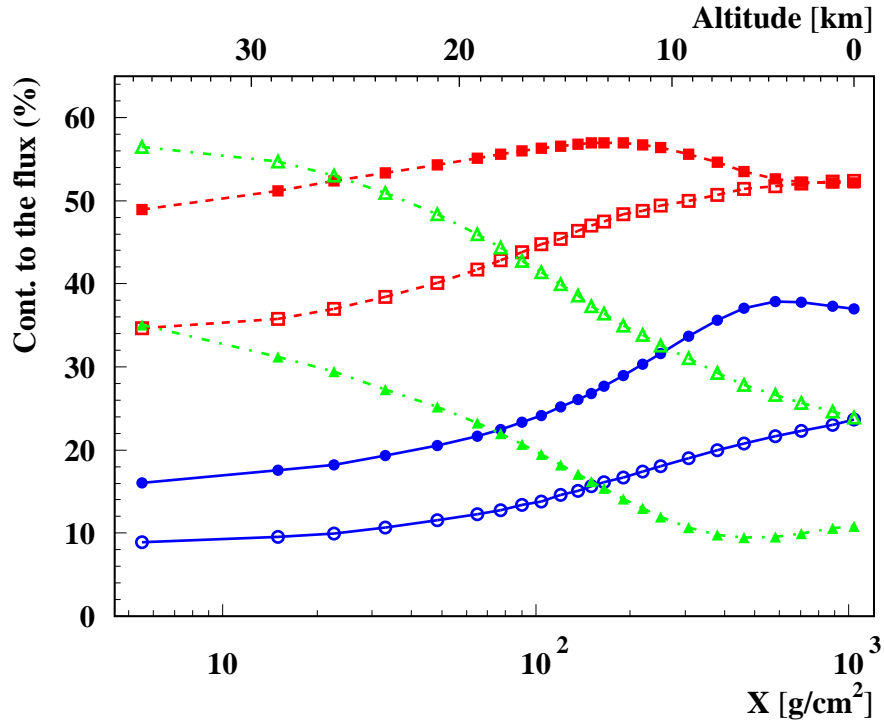


Figure 5: Relative contribution of primaries with different zenith angles to the full muon flux as function of atmospheric depth and altitude above sea level. For zenith angle: $\Theta < 30^\circ$ (circles), $30^\circ < \Theta < 60^\circ$ (square), $60^\circ < \Theta$ (triangle). The solid (open) symbols correspond to all muons (muons with momentum greater than 10 GeV/c). The lines are drawn to guide the eye.

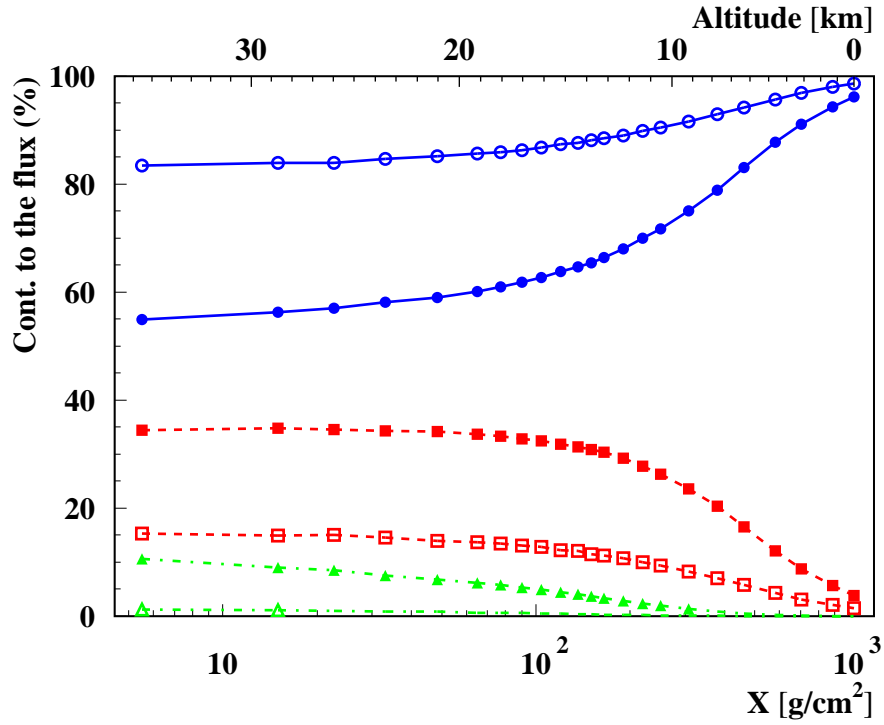


Figure 6: Relative contribution of primaries with different zenith angles to the flux of quasi-vertical muons as function of atmospheric depth and altitude above sea level. For zenith angle: $\Theta < 30^\circ$ (circles), $30^\circ < \Theta < 60^\circ$ (square), $60^\circ < \Theta$ (triangle). The solid (open) symbols correspond to all muons (muons with momentum greater than $1 \text{ GeV}/c$). The lines are drawn to guide the eye.

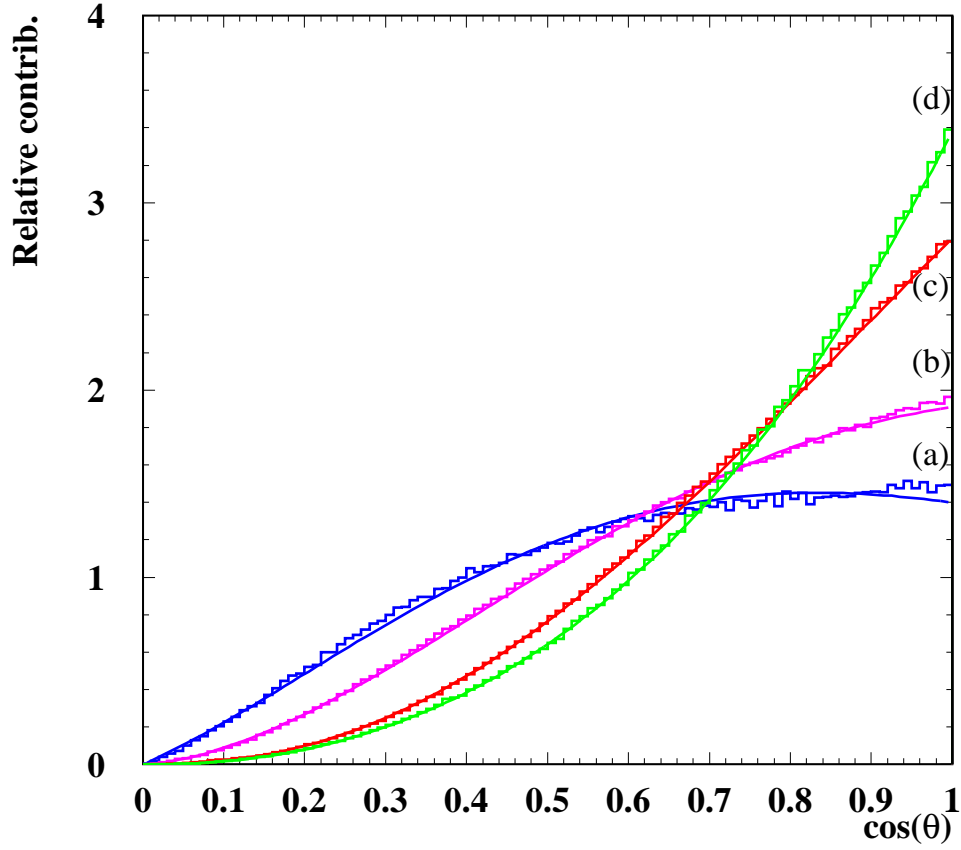


Figure 7: Normalized angular distributions of muons versus the cosine of the arrival zenith angle for several atmospheric depths: (a) 5.5 g/cm^2 , (b) 77 g/cm^2 , (c) 308 g/cm^2 , and (d) 885 g/cm^2 . The histograms represent the simulated data while the smooth lines correspond to fits of distribution to the form (1). 20° correspond to $\cos \theta = 0.94$.

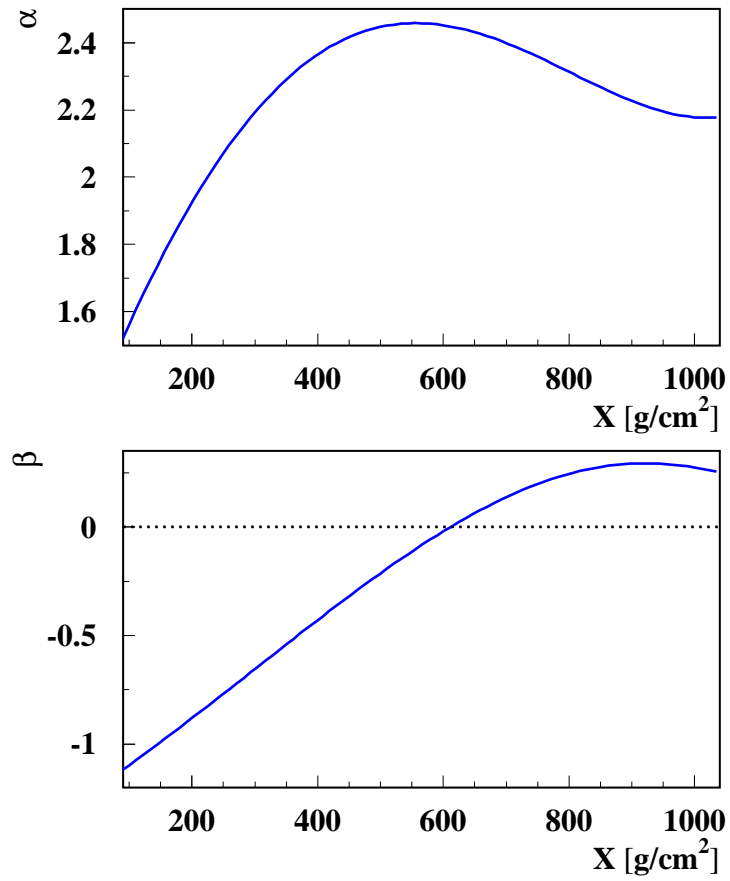


Figure 8: α and β versus atmospheric depth.

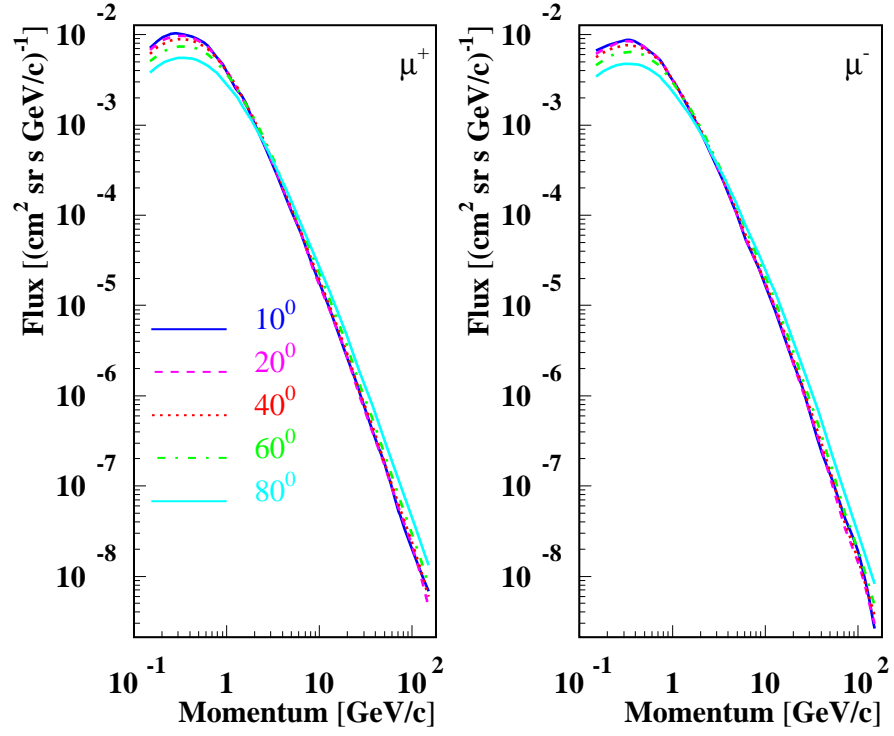


Figure 9: Simulated μ^+ and μ^- fluxes at 22.6 g/cm^2 calculated using different acceptance cones, plotted versus muon momentums.

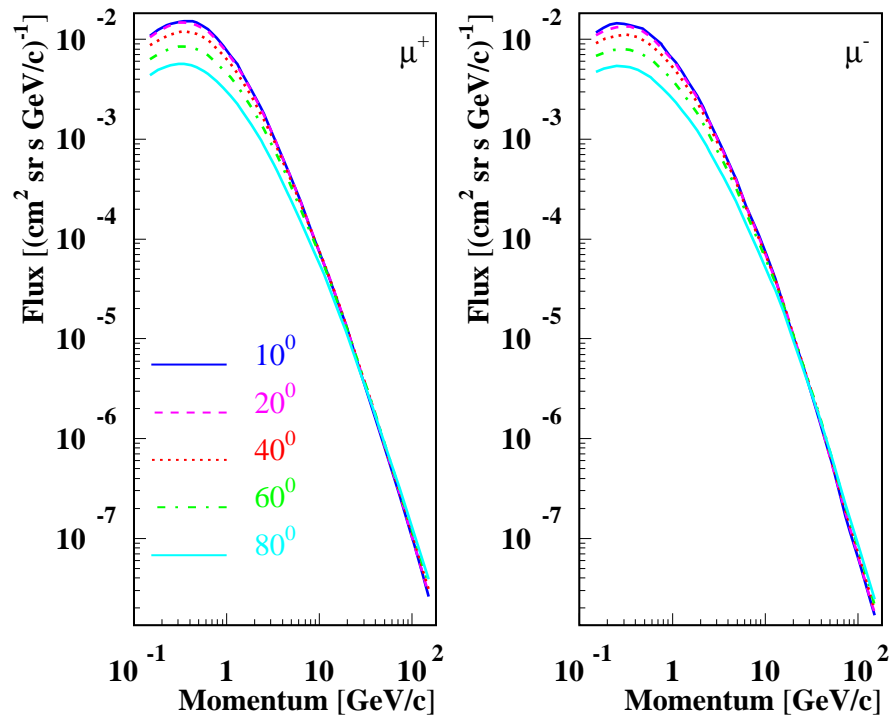


Figure 10: Same as figure 9, but for $x = 308 \text{ g/cm}^2$

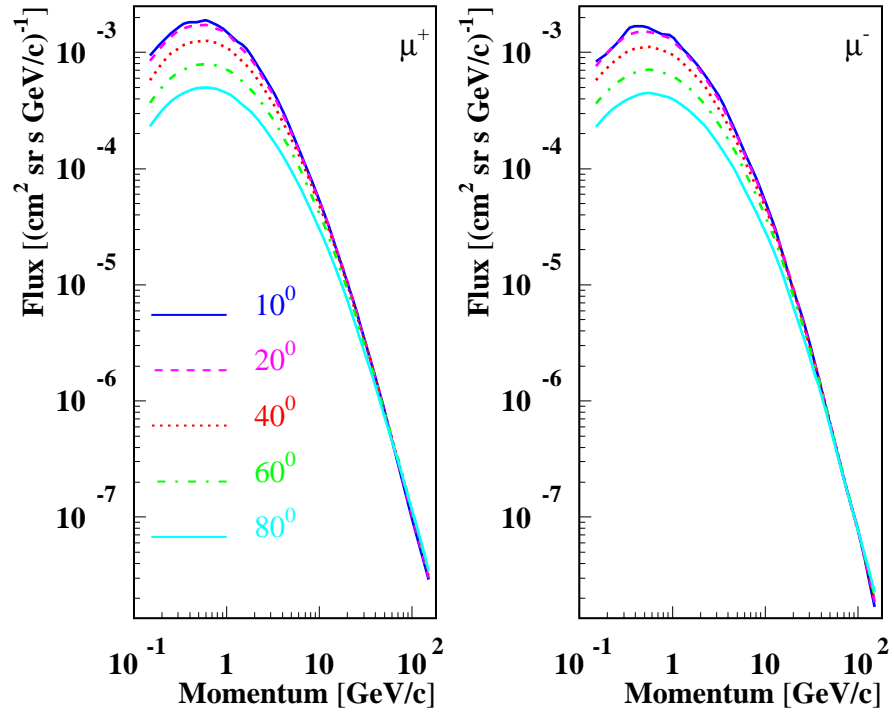


Figure 11: Same as figure 9, but for $x = 885 \text{ g/cm}^2$

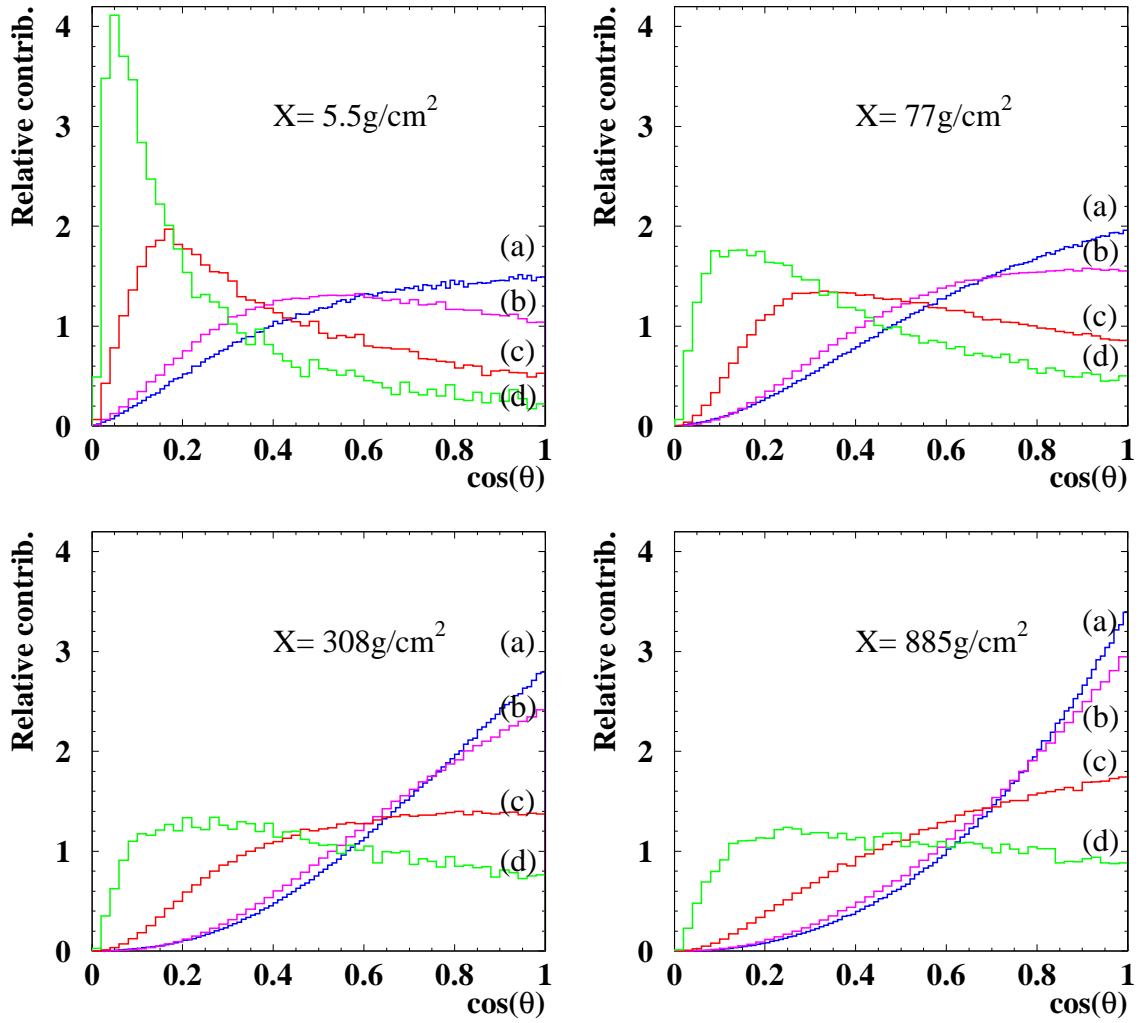


Figure 12: Normalized angular distributions of muons versus the cosine of the arrival zenith angle for several atmospheric depths. The different lines correspond to (a) all simulated muons, (b) $p_\mu > 1 \text{ GeV}/c$, (c) $p_\mu > 10 \text{ GeV}/c$, and (d) $p_\mu > 100 \text{ GeV}/c$.

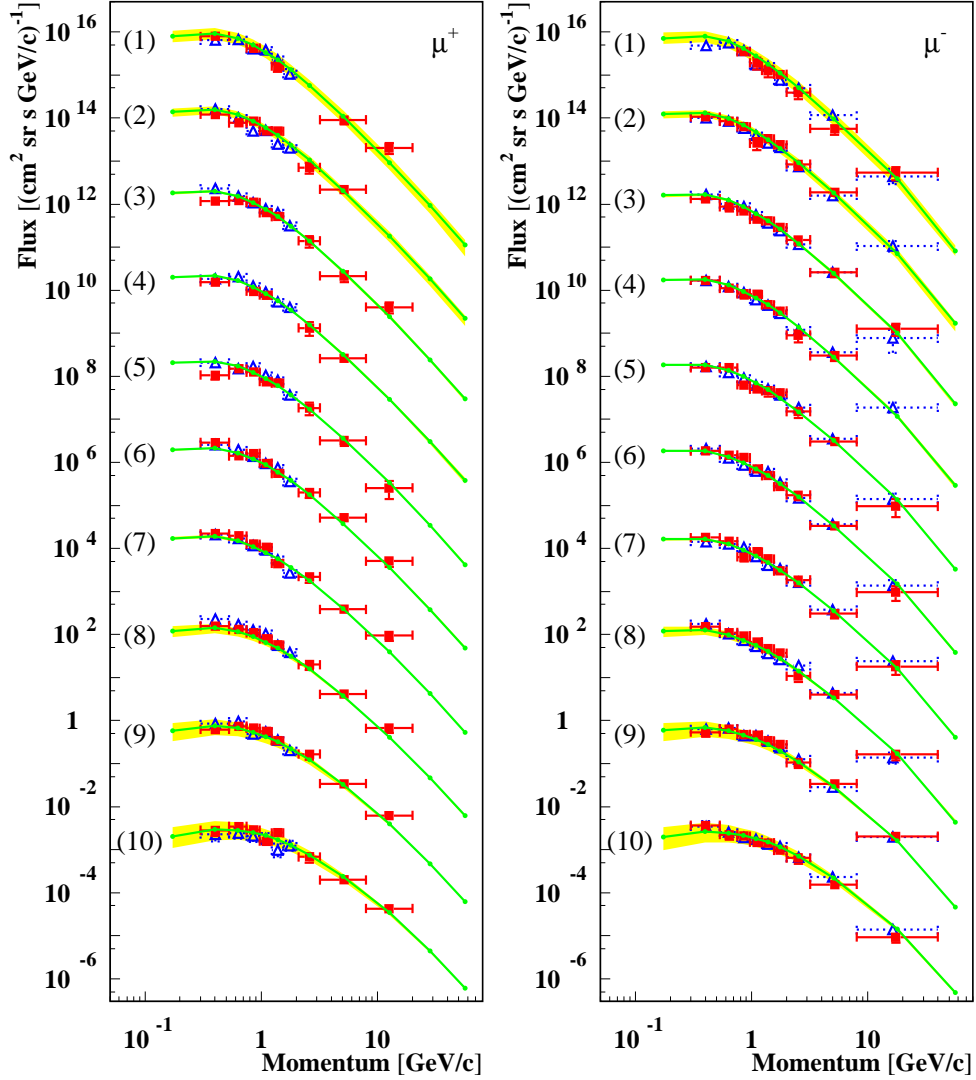


Figure 13: Absolute muon flux versus muon momentum. The solid squares (open triangles) correspond to CAPRICE98 (CAPRICE94) data. The solid lines represent the AIRES simulations at the respective average depths. The shaded areas indicate the variations registered in the simulated flux when passing from the minimum to the maximum depth of the corresponding measurement interval. Different curves represent different altitudes: (1) 22.6 g/cm², scaled by 10¹⁸. (2) 48.4 g/cm², scaled by 10¹⁶. (3) 77 g/cm², scaled by 10¹⁴. (4) 104 g/cm², scaled by 10¹². (5) 136 g/cm², scaled by 10¹⁰. (6) 165 g/cm², scaled by 10⁸. (7) 219 g/cm², scaled by 10⁶. (8) 308 g/cm², scaled by 10⁴. (9) 462 g/cm², scaled by 10². (10) 704 g/cm², scaled by 1.

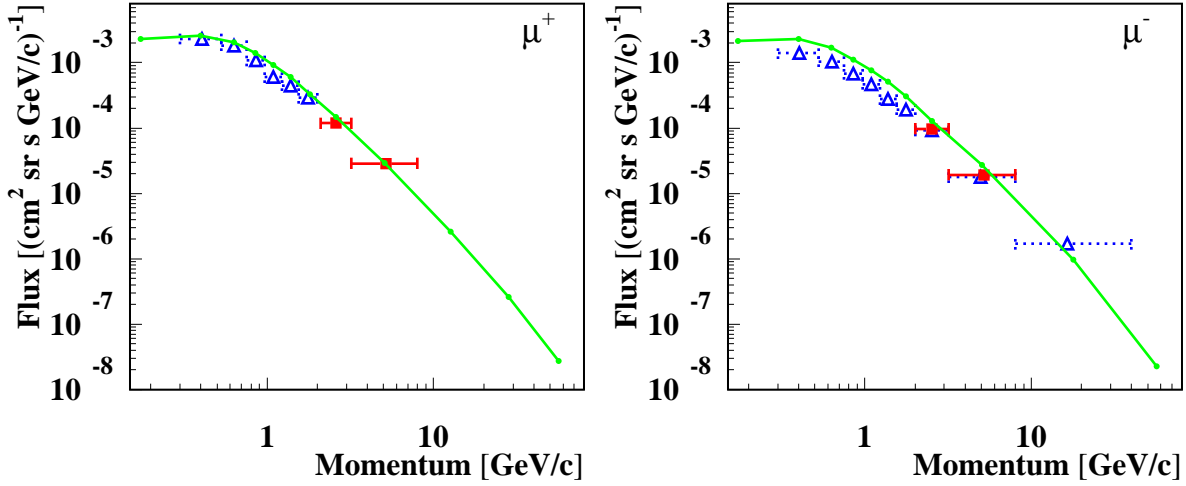


Figure 14: Absolute muon flux versus muon momentum at float altitude. The solid squares (open triangles) correspond to CAPRICE98 (CAPRICE94) data. The solid lines represent the AIRES simulations.

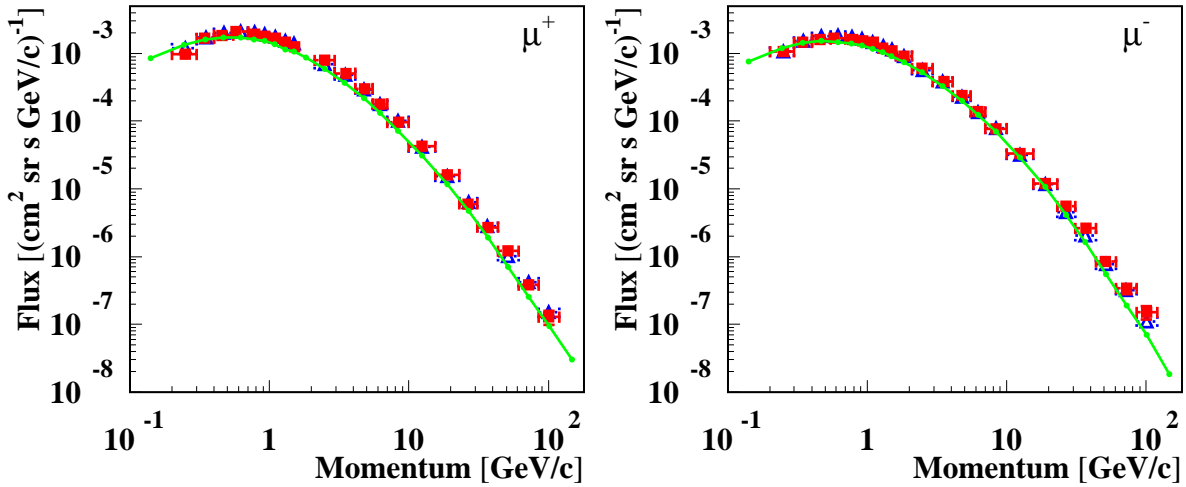


Figure 15: Absolute muon flux versus muon momentum at ground altitude. The solid squares (open triangles) correspond to CAPRICE98 (CAPRICE97) [36] data. The solid lines represent the AIRES simulations.

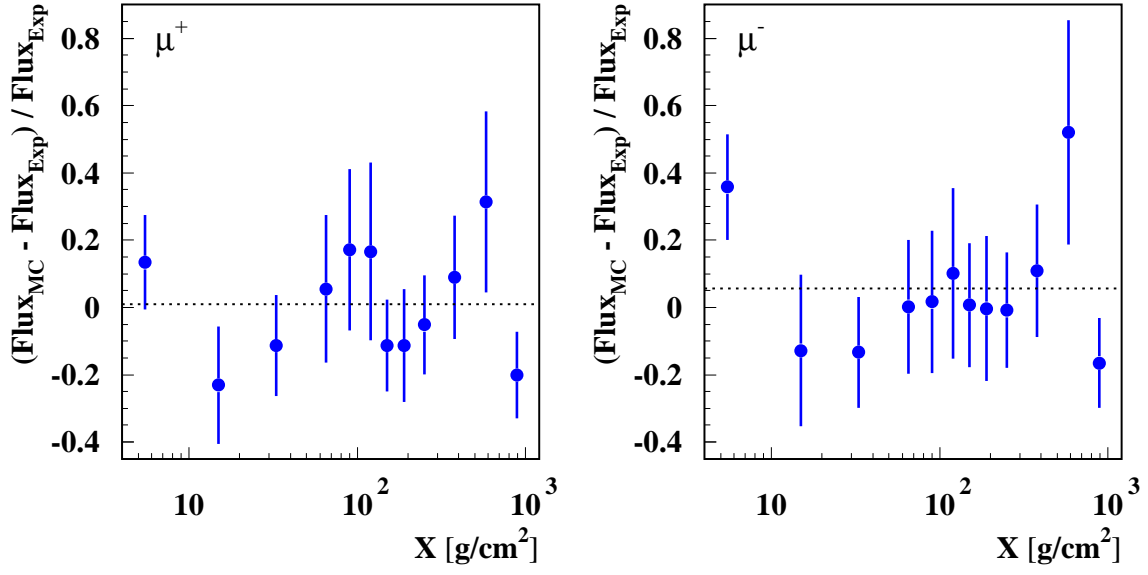


Figure 16: Relative difference simulation-experiment versus atmospheric depth. Each point corresponds to a weighted average for all rigidity bins at the respective measurement level. The dotted line represents the global average over all the considered altitudes.

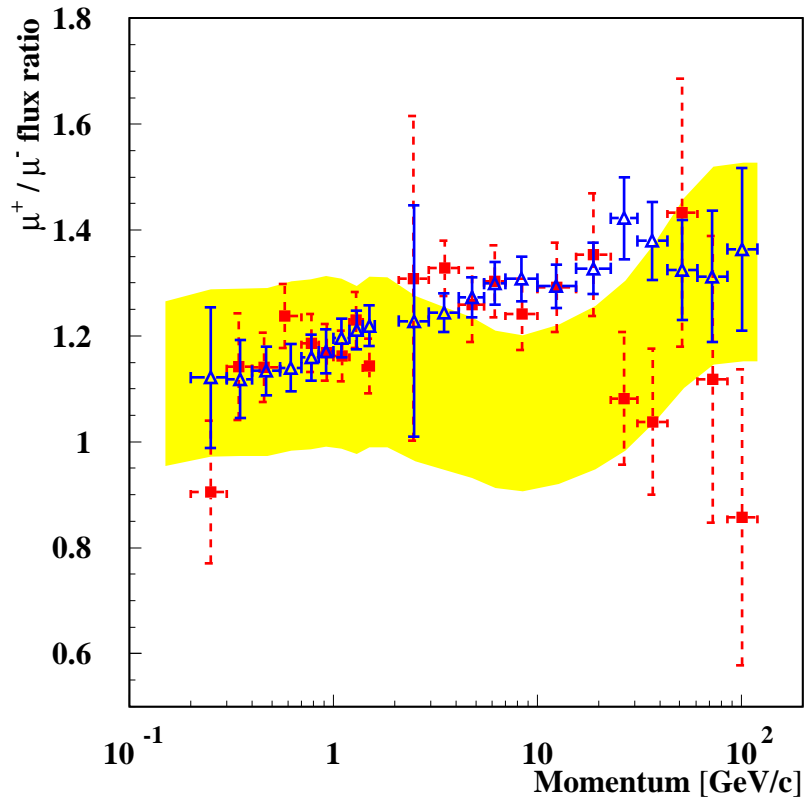


Figure 17: μ^+/μ^- flux ratio versus muon momentum, at ground altitude. The squares (triangles) correspond to CAPRICE98 (CAPRICE97) data. The shaded area corresponds to the simulations taking into account an estimation of the modelling errors.

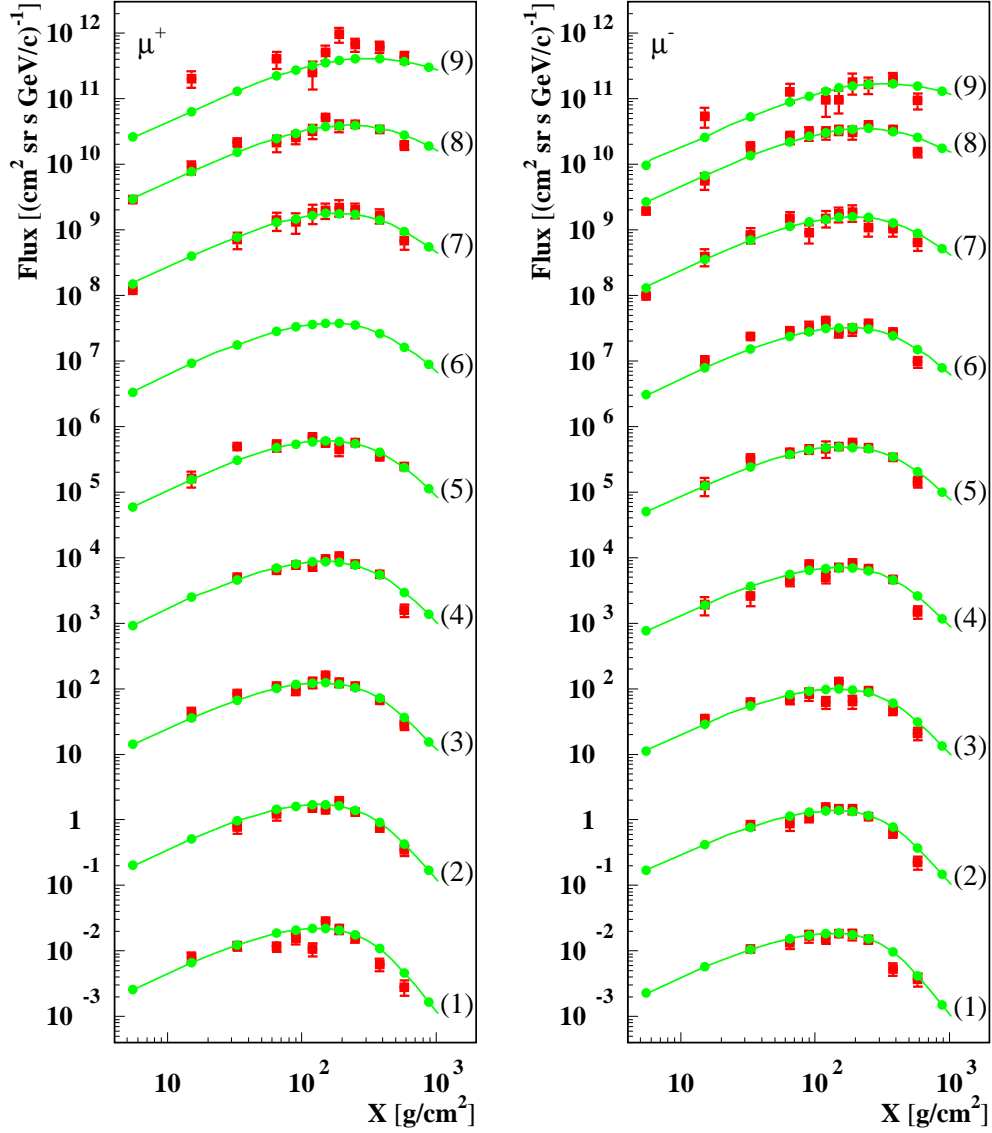


Figure 18: Absolute muon flux versus atmospheric depth. The squares represent CAPRICE98 data, while the solid lines correspond to the simulations with AIREs. Different curves represent different momentum bins (in GeV/c); for μ^+ (μ^-): (1) 0.3 – 0.53, (0.3 – 0.53) scaled by 1. (2) 0.53 – 0.75, (0.53 – 0.75) scaled by 10^2 . (3) 0.75 – 0.97, (0.75 – 0.97) scaled by 10^4 . (4) 0.97 – 1.23, (0.97 – 1.23) scaled by 10^6 . (5) 1.23 – 1.55, (1.23 – 1.55) scaled by 10^8 . (6) 1.55 – 2.1, (1.55 – 2.0) scaled by 10^{10} . (7) 2.1 – 3.2, (2.0 – 3.2) scaled by 10^{12} . (8) 3.2 – 8, (3.2 – 8) scaled by 10^{14} . (9) 8 – 20, (8 – 40) scaled by 10^{16} .